



This is a repository copy of *Top-of-rail friction modifier performance assessment: high pressure torsion testing; creep force modelling and field validation*.

White Rose Research Online URL for this paper:

<https://eprints.whiterose.ac.uk/202343/>

Version: Published Version

---

**Article:**

Evans, M.D., Lee, Z.S., Harmon, M. et al. (5 more authors) (2023) Top-of-rail friction modifier performance assessment: high pressure torsion testing; creep force modelling and field validation. *Wear*, 532-533. 205073. ISSN 0043-1648

<https://doi.org/10.1016/j.wear.2023.205073>

---

**Reuse**

This article is distributed under the terms of the Creative Commons Attribution (CC BY) licence. This licence allows you to distribute, remix, tweak, and build upon the work, even commercially, as long as you credit the authors for the original work. More information and the full terms of the licence here:

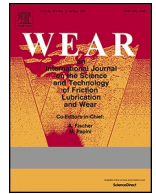
<https://creativecommons.org/licenses/>

**Takedown**

If you consider content in White Rose Research Online to be in breach of UK law, please notify us by emailing [eprints@whiterose.ac.uk](mailto:eprints@whiterose.ac.uk) including the URL of the record and the reason for the withdrawal request.



[eprints@whiterose.ac.uk](mailto:eprints@whiterose.ac.uk)  
<https://eprints.whiterose.ac.uk/>



## Top-of-rail friction modifier performance assessment: High pressure torsion testing; creep force modelling and field validation

M.D. Evans<sup>a</sup>, Z.S. Lee<sup>a</sup>, M. Harmon<sup>a</sup>, K. Six<sup>b</sup>, A. Meierhofer<sup>b</sup>, R. Stock<sup>c,1</sup>, D.V. Gutsulyak<sup>d</sup>, R. Lewis<sup>a,\*</sup>

<sup>a</sup> The University of Sheffield, Department of Mechanical Engineering, Mappin Street, Sheffield, S1 3JD, UK

<sup>b</sup> Virtual Vehicle Research GmbH, Inffeldgasse 21, 8010, Graz, Austria

<sup>c</sup> Plasser Canada Inc., 2705 Marcel Street, Montreal, QC, Canada

<sup>d</sup> L.B. Foster, Burnaby, British Columbia, Canada

### ARTICLE INFO

#### Keywords:

Top-of-rail friction modifiers  
Wheel/rail interface  
HPT testing

### ABSTRACT

Top-of-Rail products that give intermediate friction offer many benefits when applied to the wheel/rail interface. Water-based top-of-rail friction modifiers (TOR FMs), have been shown to reduce energy consumption, wear, noise, corrugation and rolling contact fatigue. This work was aimed at developing a test approach, based on the High Pressure Torsion (HPT) method, that allowed an improved assessment of their performance over those that recycle constantly over the same test surface. The outputs would then be used to parameterise the Extended Creep Force (ECF) model to enable full-scale predictions to be made that could be compared with field measurements of wheel/rail interface friction.

The HPT method developed used representative amounts of product based on assessment of wayside and on-board application rates. Friction levels achieved matched those expected for intermediate levels. The friction level was sensitive to the amount applied though. The parameterised ECF model was able to predict friction levels that matched those from the field very closely. A framework for using friction measured in small-scale tests has been developed that could now be applied to other third body materials for making valid predictions of full-scale performance.

### 1. Introduction

The benefits of water-based top-of-rail friction modifiers (TOR FMs) have been widely studied in the laboratory and the field. The benefits are chiefly reduced energy consumption [1], noise [2–6], wear (through separation of contacting surfaces and friction reduction as well as through lateral force reduction) [7–14], corrugation [15–17] and rolling contact fatigue (RCF) [18,19]. Additionally, they have been shown to have no negative effects on traction and braking [4,20] or track isolation [21].

However, there has been little focus on incorporating the effects of TOR FMs on friction into multi-body dynamic simulations to better understand their effects on train performance. If this is achieved, then they could be considered in costing tools such as the Vehicle Track Interaction Strategic Model (VTISM) used in the UK helping suppliers and users to make better business cases for their introduction [22]. One

way this could be achieved is to develop an approach for predicting creep force behaviour for a wheel/rail interface with a TOR product applied. This could then be implemented in a multi-body dynamics simulation of a train on track to understand how they affect forces in the contact patch. The creep force relationships and wheel/rail contact forces could then also be fed into wheel and rail damage models.

The aim of this work was to: use a high pressure torsion (HPT) test approach [23] to characterise TOR FM layers; parameterise the Extended Creep Force (ECF) model using the resulting data; use the updated ECF model to predict full-scale wheel/rail interface behaviour and then finally validate these predictions against locomotive field data. The ECF model output will then be used in the future to feed into multi-body dynamic simulations and wheel and rail damage models.

\* Corresponding author.

E-mail address: [roger.lewis@sheffield.ac.uk](mailto:roger.lewis@sheffield.ac.uk) (R. Lewis).

<sup>1</sup> formerly L.B. Foster, Burnaby, BC, Canada.

## 2. Background

A TOR product is applied to the top of the rail to reduce the friction coefficient from dry values to an intermediate value in the range 0.2–0.4. Fig. 1 shows a graph adapted from previous work to define top-of-rail product performance expectations that indicates friction regimes for the wheel/rail interface as well as how applied products will alter the friction level [24]. Various types of TOR product are used. The focus in this work was on a TOR friction modifier (TOR FM), which is water based. A TOR FM is made up of solid particles in a water-based suspension. It can be applied to the rail from wayside applicators which pump a puddle of product onto the rail head, or through on-board systems that spray the product directly onto the rail or wheel tread. The water evaporates, leaving behind the solid particles to mix with the existing third body layer on the surface of the wheel/rail. There are solid stick varieties that are applied directly to the wheel using a spring system. They should not be confused with other top of rail products such as top-of-rail lubricants (oil or grease based products) or hybrid products [24].

Field testing to fully characterise TOR FM friction behaviour and generate creep curves is prohibitively expensive and does not allow for precise control over all the factors that can influence results, therefore laboratory tests are required. There are numerous types of laboratory tests that have been used to explore friction characteristics of TOR FMs. The most popular are twin-disc set-ups [14,18,21,25] or full-scale wheel-rail test facilities [26–28].

Optical apparatus using a driven ball-on-flat set-up has been used for film thickness measurements [29] and mini-traction machines have used the same approach for friction measurements. These rigs have small contacts which can present an issue, but are good for examining at high resolution the differences seen with changes in product formulation [7, 8,10].

Most small-scale test approaches result in the same “wheel” running over the same “rail” so there is constant recycling of the product/third body layer and they are therefore not representative of field operation. Additionally, various test runs at several discrete levels are required to build an entire creep curve. Tests have been run where slip has been changed continuously to measure a creep curve, but due to the product consumption it is hard to determine then if the friction has changed due to varying slip or due to less product being present in the contact [30]. An issue in previous work has been that the amount of product has not been scaled appropriately from the amounts present in the actual wheel/rail contact from wayside or on-board application. As will be seen later, amounts needed are very small. In terms of thickness for a puddle applied wayside this will be approximately 10 μm and for on-board 0.025 μm. This will be a key issue addressed in this work as product performance is very sensitive to amount applied as shown in the field tests carried out by Davis [31], as shown in Fig. 2.

HPT testing has been developed to measure the shear stress between

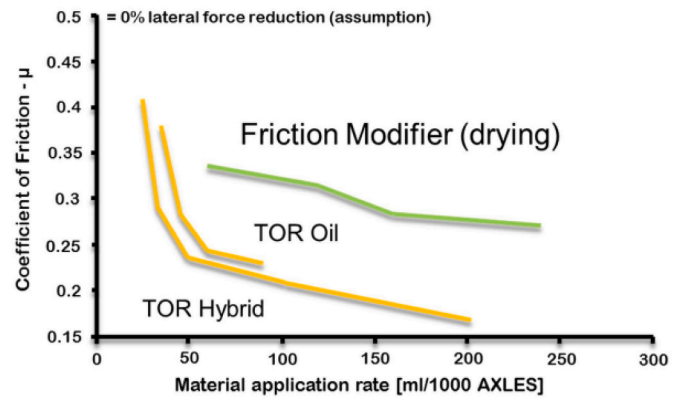


Fig. 2. Performance of different TOR Products from Field Measurements [31].

two specimens [23]. This initial commissioning work modified the specimen geometry, developed a run-in procedure and test progression method to produce consistent and repeatable results. It has further been used to analyse the effect different sands have on traction under dry, wet and leaf contaminated conditions [32]. More recently, it has been used to further understand by testing with different amounts of water and iron oxide [33] and TOR products [34]. This test method has the advantage that an entire torque (or shear stress) over rotation angle (displacement at mean radius) curve can be generated with less than one rotation. This method measures the torque required to sustain the rotation of two specimens with an annulus contact. The shear stress in the contact can then be calculated which provides characterisation of the friction of the interface. Although this test is not fully representative of the wheel-rail contact it provides information on the characteristics of the third body layer to use as inputs for a creep force model as will be explained later. In this work the aim was to use the method to characterise the interface performance with different levels of TOR FM applied.

Recent reviews [35,36] evaluated different creep force models that could incorporate third-body layers. These highlighted benefits of the ECF model in representing the behaviour of the wheel/rail contact when contamination or applied products are present. The ECF model, which is described in detail in previous publications [37,38], builds on a creep force model developed by Tomberger et al. [39] which is an extension of Kalker’s FASTSIM [40]. Using output data from HPT tests, a framework has been described that allows parameterisation of the ECF model for different types of third-body material (liquid or solid) [23]. This can then be used for making predictions of the full-scale contact behaviour.

The ECF model (see Fig. 3) output is the creep force behaviour in the wheel/rail interface (see bottom left sub-plot). It works on the premise that there is always a third-body layer present. With no product being applied this is made up from wear debris and oxides etc. (see top left hand sub-plot). “Real” third-body layers (from addition of top-of-rail product, sand or water) can be accommodated along with the effects of roughness and the “tribological” plasticity phenomena in the near surface layers of wheel and rail materials [41]. The wheel and rail are assumed to behave elastically. Elastic-plastic behaviour, though, is taken for the third-body layer. Voce’s hardening law [42] is used to describe this, where contact pressure and temperatures dependency is considered (see top right sub-plot). HPT test output can be used to parameterise the third-body layer model. The third-body layer model is implemented as a brush model for rolling contacts (bottom right sub-plot) to predict the creep force behaviour.

## 3. Laboratory experimental details

### 3.1. HPT test apparatus

The HPT test uses a servo-hydraulic test platform. A hydraulic

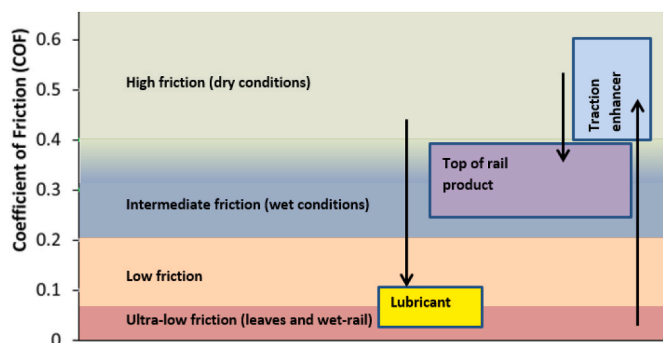


Fig. 1. Wheel/rail friction range and effect of applied products (adapted from Ref. [24]).

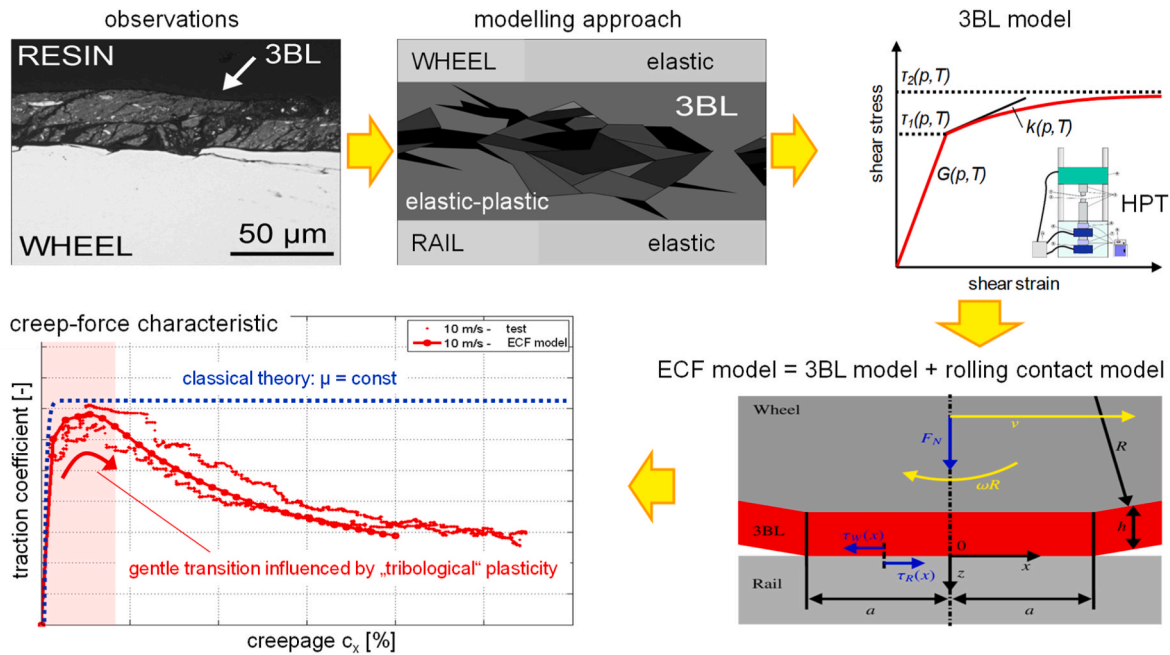


Fig. 3. ECF model: approach and methodology [23].

actuator provides the normal force to the specimens with two Linear Variable Differential Transformers (LVDTs) measuring displacement in axial and torsional directions and a load cell to record the normal and torque forces.

At higher radii in the HPT contact interface, the same creep stress will have a greater contribution to the torque supported. Therefore, an average creep stresses across the contact patch is calculated. The midpoint radius cannot be used to calculate the creep stress from the measured torque so a value known as the “effective radius of friction” (ERF) is defined instead as the point at which creep stress is to be calculated:

$$ERF = \frac{2}{3} \frac{(R_o^3 - R_i^3)}{(R_o^2 - R_i^2)} \quad (1)$$

where  $R_o$  is the outer radius of the contact and  $R_i$  is the inner radius of contact.

Until the contact reaches full sliding, the elements at higher radii will have displaced further and therefore be more highly stressed than those at lower radii; for this reason, only an average creep stress can be

calculated from the measured torque.

The HPT test apparatus is shown schematically in Fig. 4. The specimens consist of an upper annulus specimen made from wheel material (R8T) and a lower flat, square specimen made from rail material (R260). These are both ground to achieve an Ra of 0.5 μm. The specimens are compressed together, creating an annulus contact (area 168 mm<sup>2</sup>). The test apparatus maintains a steady load to produce the desired contact pressure and rotates the specimens (<1 mm/s) relative to each other at a constant angular velocity. Before each test (and for this case prior to the third-body layer being created) the disc surfaces were “run-in” using the procedure described in the development work [23], where more details on all aspects of the technique can be found.

### 3.2. Generating TOR FM layers

To generate a TOR FM layer on the surface of the lower specimen appropriate amounts must be applied. In order to replicate the very tiny amounts of product that are active in the wheel/rail interface from the total amount in the puddle deposited on the rail head from a wayside applicator, the TOR FM must be diluted as the very small quantities are

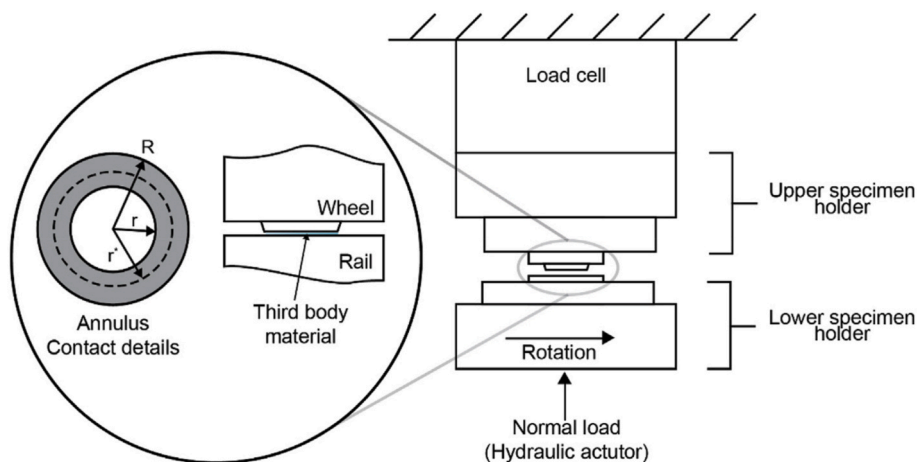


Fig. 4. Schematic of HPT configuration,  $r = 5.25$  mm,  $R = 9$  mm [32].

hard to apply evenly to the surface. Typical field application rates are shown in Table 1. The TOR FM was diluted with distilled water to produce the required concentration. The water was then evaporated to leave the solid constituent of the TOR FM which forms a third-body layer on the rail specimen in the HPT test rig comparable to field application.

The following procedure was used to apply the TOR FM dilutions to the lower specimen surface.

- Specimens were cleaned with acetone
- Rubber washers were placed on the specimens to provide the known application area
- 400  $\mu\text{L}$  of the TOR FM dilution was applied
- Specimens were placed in vacuum oven to allow evaporation without oxidation
- Once evaporation had taken place, the specimens were removed from the oven and stored in dry conditions

### 3.3. Test conditions and methodology

The test procedure was as follows.

- Specimens were installed in the test machine taking care not to contaminate the contacting surfaces
- Specimens were brought into contact at the set normal pressure
- Specimens were rotated by the equivalent of 0.4 mm at the effective radius of friction relative to each other
- Specimens were brought out of contact

MATLAB scripts are used to extract, process and plot the data.

Fresh discs were used for each contact condition, but conditions were repeated multiple times without changing specimens. Five different TOR FM amounts were tested representing the amounts used in service: 16, 32, 64, 512, 2048 mL/mile. They were tested at 600 MPa contact pressure and compared to a dry baseline. Sixteen repeats using the same specimens were tested to get information about the consumption behaviour of the product. Additional runs of over-applied neat (undiluted) TOR FM, dried and wet were also tested at 900 MPa to understand the effects of a gross “over-application” of TOR FM.

## 4. HPT results

Fig. 5 shows the results from the five different TOR FM dosages compared to a dry baseline. Only the first three runs are presented here for clarity of the graph (these are repeat cycles on the same surface). It shows that applying TOR FM reduces the shear stress (and hence friction

**Table 1**

Typical field application amounts and dilution factors needed to achieve them for this study.

Dosing (mL/mile)	TOR FM per unit area ( $\mu\text{L}/\text{mm}^2$ )	Product to be applied to 573 $\text{mm}^2$ ( $\mu\text{L}$ ) (area of bottom specimen)	Dilution factor for 400 $\mu\text{L}$ application	Relevance to field application
16	0.0002	0.11	3490	TOR FM On-Board system testing value
32	0.0004	0.23	1750	TOR FM On-Board system testing value
64	0.0008	0.46	872	TOR FM On-Board system testing value
512	0.0064	3.7	108	Representative value for wayside application supplied by TOR FM applicator supplier
2048	0.0256	14.7	26.3	Included to investigate the effect of over-application

coefficient). Increasing the dosage amount decreases the shear stress further until the 512 mL/mile dosage amount when an increase in application does not decrease the shear stress any further. Figs. 6 and 7, which contain the 16 mL/mile and 23 mL/mile dosage results respectively, show that as TOR FM is consumed during subsequent test runs, shear stress steadily increases. In Fig. 8, the 64 mL/mile dosage shows no increase in shear stress during the sixteen test runs. This relationship was seen for the higher dosage amounts as well.

Fig. 9 summarises the results seen in Figs. 5–8. It should be noted here that in Fig. 9A, the “0” mL/mile data point was actually for distilled water application which means that there was a third-body layer present, but no TOR FM. This graph shows the initial shear stress/traction coefficient for a particular condition. Fig. 9B differs in that it shows the maximum values for each run. Fig. 9A shows how the shear stress drops from the “dry” value when TOR FM is applied up to a point where increasing application does not result in a decrease in shear stress. Fig. 9B shows how the shear stress evolves as the sixteen test runs are completed for all the dosage levels. For the 16 mL/mile dosage, the shear stress rises and levels off near to the dry values. The 32 mL/mile dosage also increases, but not at the same rate and is still rising at the end of the sixteen test runs. For all higher dosage amounts, there is no increase in shear stress as the number of test runs increases. It is hypothesised that if the number of test runs is increased, all the dosages will eventually exhibit the same behaviour as the 16 mL/mile dosage. These relationships are logical as the greater the amount of TOR FM in the contact, the longer it will take to be consumed.

Fig. 10 shows the test specimens at the end of the test for each of the dosage amounts. There is a clear progression in the amount of damage seen from the high dosage specimens to the low dosage specimens. For the 16 mL/mile specimens (Fig. 10A) almost all the contact area is damaged as the TOR FM has been consumed. The surfaces look very similar to those from dry tests [23]. This is seen by the rise in shear stress in Fig. 9. For the 32 mL/mile specimens (Fig. 10B), damage is concentrated to the edges, caused by the sliding distance being largest here, resulting in more extreme conditions at the edges. For the higher dosage amounts there is increasing amount of TOR FM remaining on the specimens at the end of the test and therefore it is still providing lower shear stress than dry values as seen in Fig. 9.

Tests were also completed with over-application of TOR FM, both dried and wet. Fig. 11 shows that the friction coefficient drops to 0.05, lower than the minimum seen in previous presented tests. The friction coefficient is the same for both wet and dry cases, but the shape of the initial curve is different. It is worth noting that if a real wheel encounters wet TOR FM, it is likely to eject some of the product. This feature is not replicated in this test procedure.

## 5. Field testing

The field testing was carried out using the same approach used by Meierhofer et al. for assessment of low adhesion conditions [43]. The tests were run at the VUZ Velim Test Centre in the Czech Republic. Two locomotives coupled together were used for the measurements. One was used to provide constant velocity for the tests. In the other the slip controller in the traction package was used to achieve slip variation on one axle. The others were in pure rolling. Negative slip was used to represent traction conditions. Rotational speed and torque were taken from the traction package and used to calculate the slip percentage. A GPS device was used to track the vehicle during the tests.

TOR FM (the same one as used in the HPT tests) was applied from an on-board application system that sprayed product in the required amounts directly onto the track. The 16 and 32 mL/mile dosages used in the HPT tests are equivalent to the 10 and 20 mL/km (16.1 and 32.2 mL/mile) dosages used in the track trials, respectively.

Results from the field tests are summarised in Fig. 12. The traction coefficient values from the field tests match those for the equivalent TOR FM application very closely. The lower friction drop at higher slip ratios

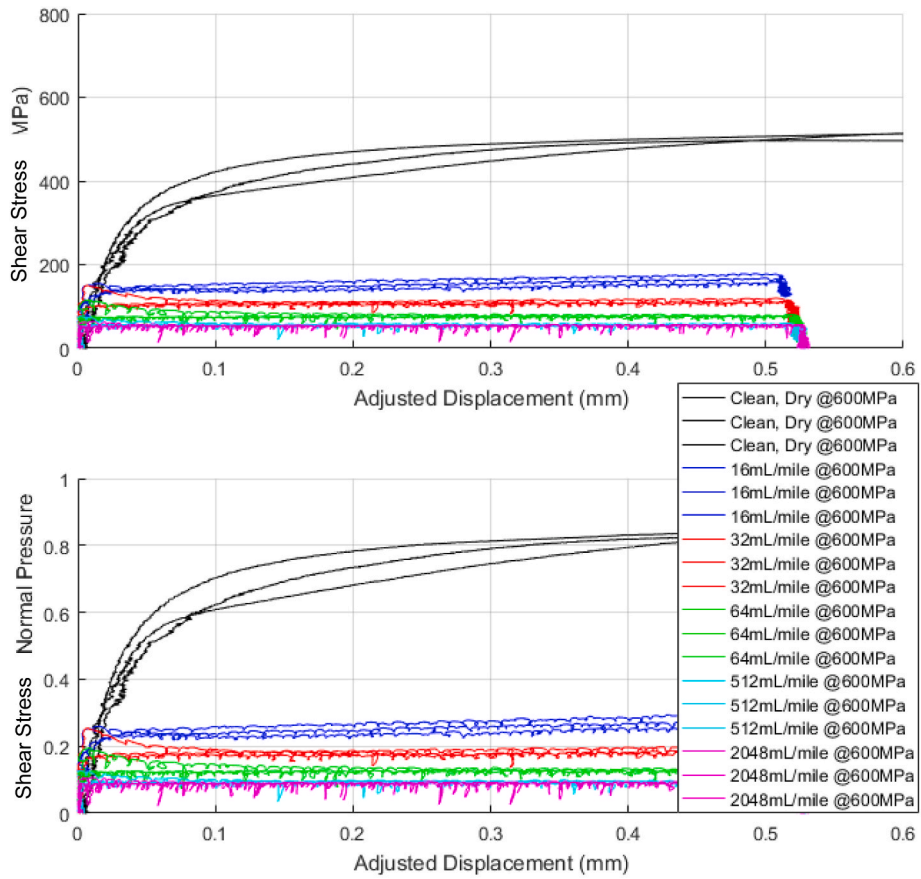


Fig. 5. Summary of first three test runs of each condition.

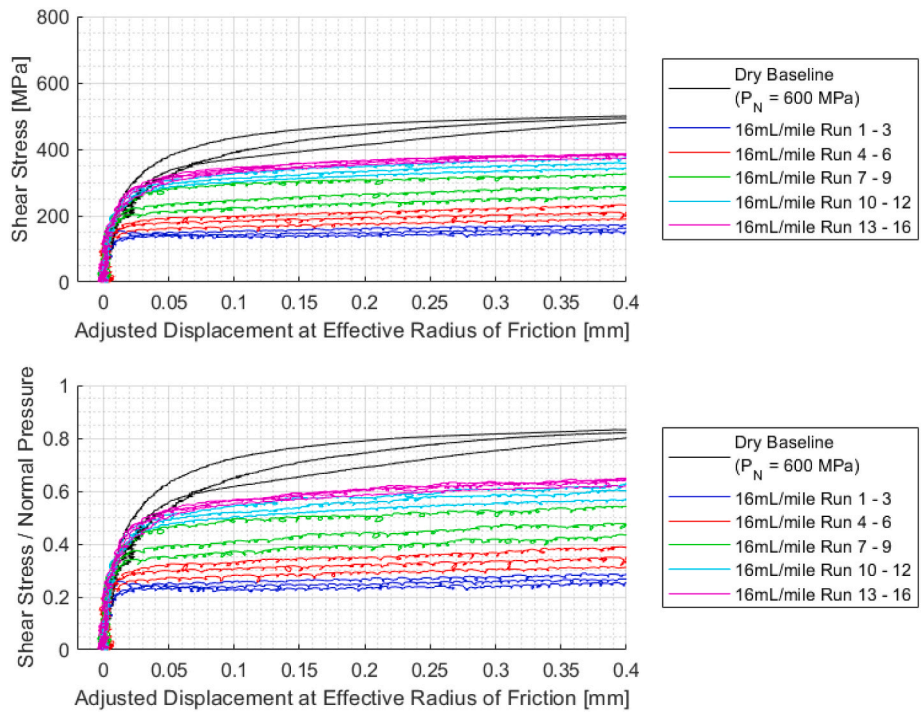


Fig. 6. Consumption of 16 mL/mile application amount for all test runs.

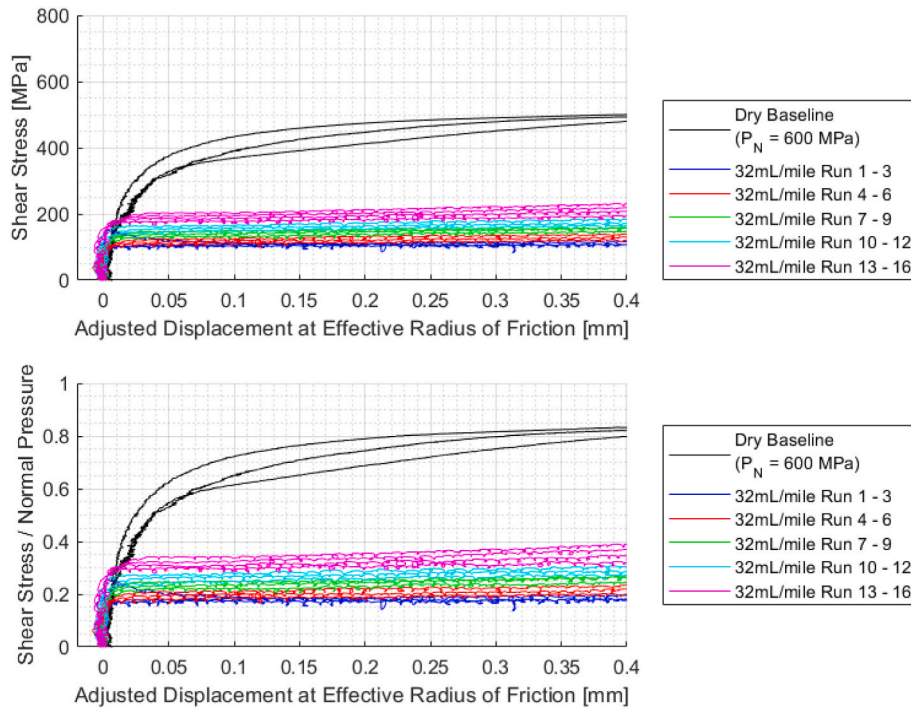


Fig. 7. Consumption of 32 mL/mile application amount for all test runs.

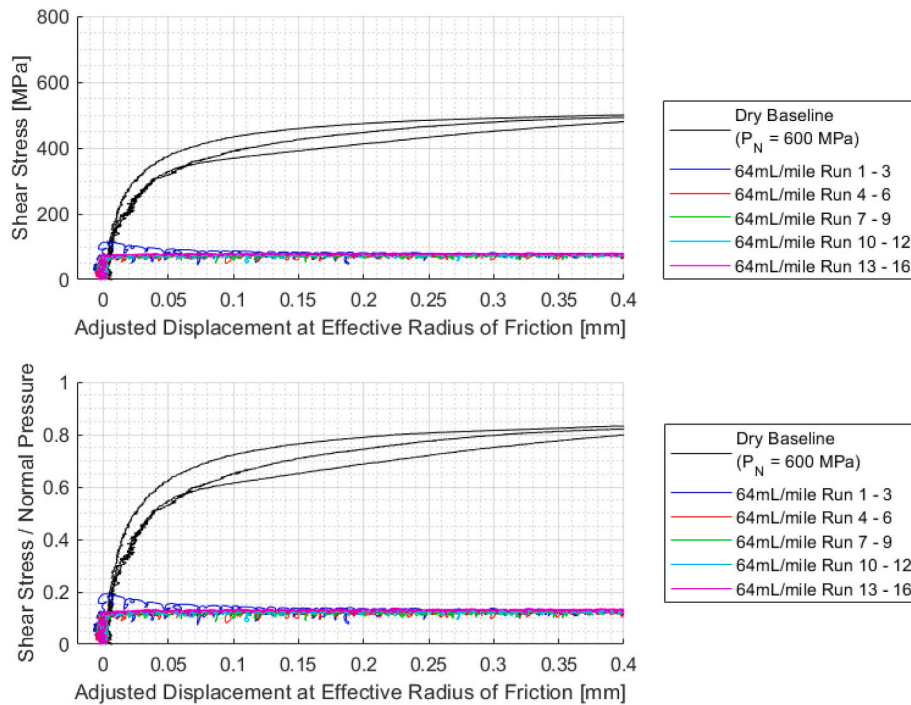


Fig. 8. Consumption of 64 mL/mile application amount for all test runs.

than the baseline supports the argument that the use of a TOR FM provides a ‘positive velocity dependant friction’ behaviour or at least closer to a ‘neutral’ behaviour. It should be noted that the tests with no product were aiming to measure “dry” conditions, but it was drizzling so it is described as a “damp” rail head. The values of friction seen for this condition reflect those seen for wet contacts in laboratory testing (0.15–0.2) [44].

## 6. ECF parameterisation and field test predictions

As mentioned in Section 2, the main innovation in the ECF model is a sub-model which implements an elasto-plastic material law, dependent on both the normal stress distribution and the local temperature to describe the behaviour of a third-body layer. Normal stresses are assumed to be Hertzian, and the local temperatures are calculated by a further sub-model.

Four material parameters are used to describe the tangential stresses

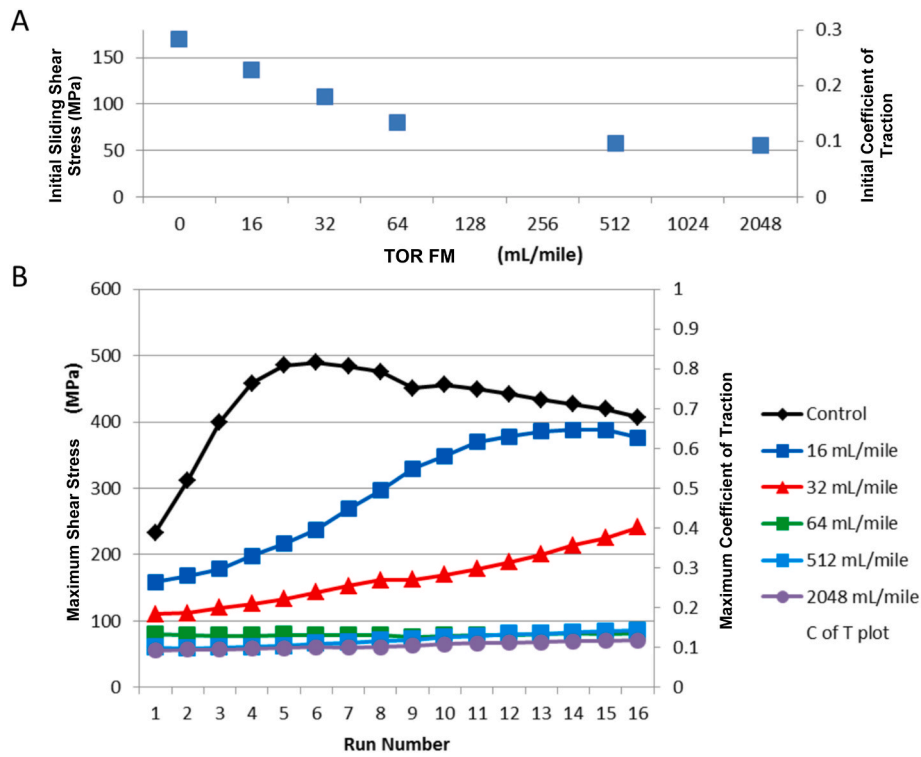


Fig. 9. Shear stress and coefficient of traction for A) the first run of each dosage B) maximum from all test runs.

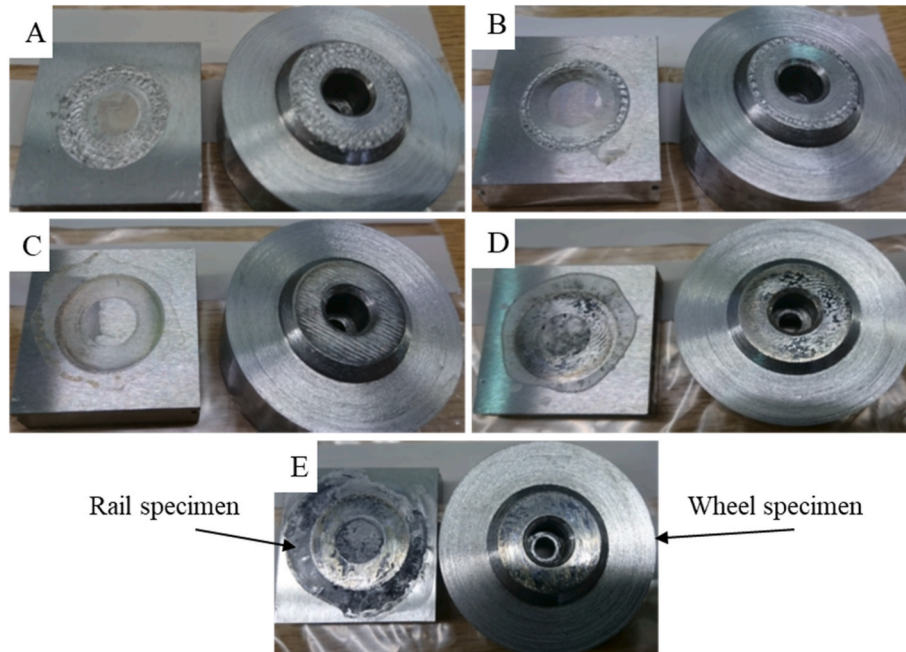


Fig. 10. Damage to specimens after 16 test runs for A) 16 mL/mile dosage B) 32 mL/mile dosage C) 64 mL/mile dosage D) 512 mL/mile dosage E) 2048 mL/mile dosage.

in a third-body layer, these are [37].

- $L_e$ : Inverted stiffness of the third body layer below the first critical shear stress
- $t_{C1}$ : First critical shear stress of the third body layer, describing the point of transition between elastic and plastic behaviour
- $L_p$ : Plasticity factor which describes the shape of the plastic shear stress behaviour between the first and second critical shear stresses

- $t_{C2}$ : Second critical shear stress of the third body layer, describing the maximum possible shear stress

Fig. 13 shows how these parameters can be gained from HPT test output [37].

Parameters  $L_e$ ,  $t_{C1}$ ,  $L_p$ ,  $t_{C2}$ , are each made up of three different parts to account for different normal stresses and local temperatures. Each parameter is made up of a nominal value, a pressure ( $p$ ) dependent value

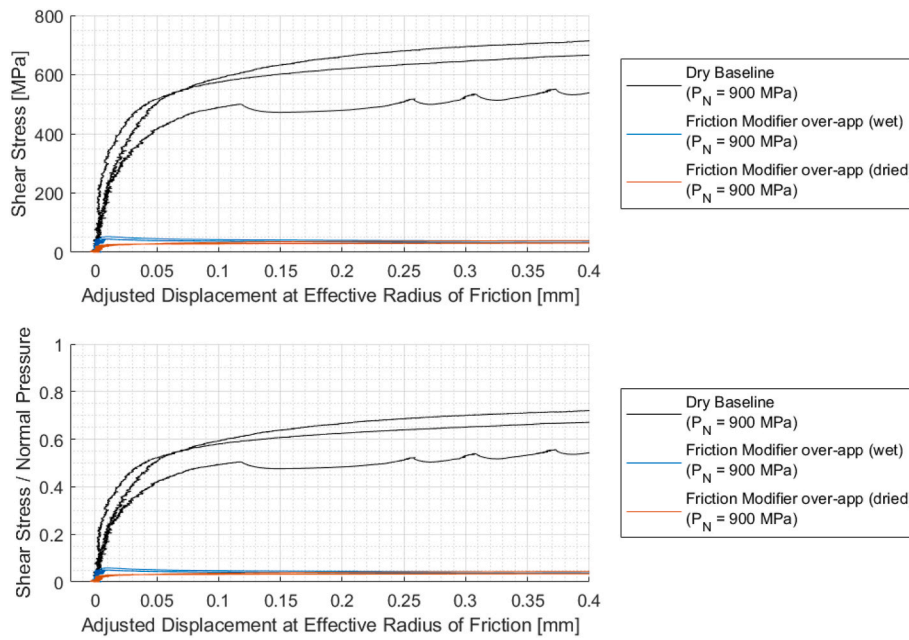


Fig. 11. TOR FM over-application.

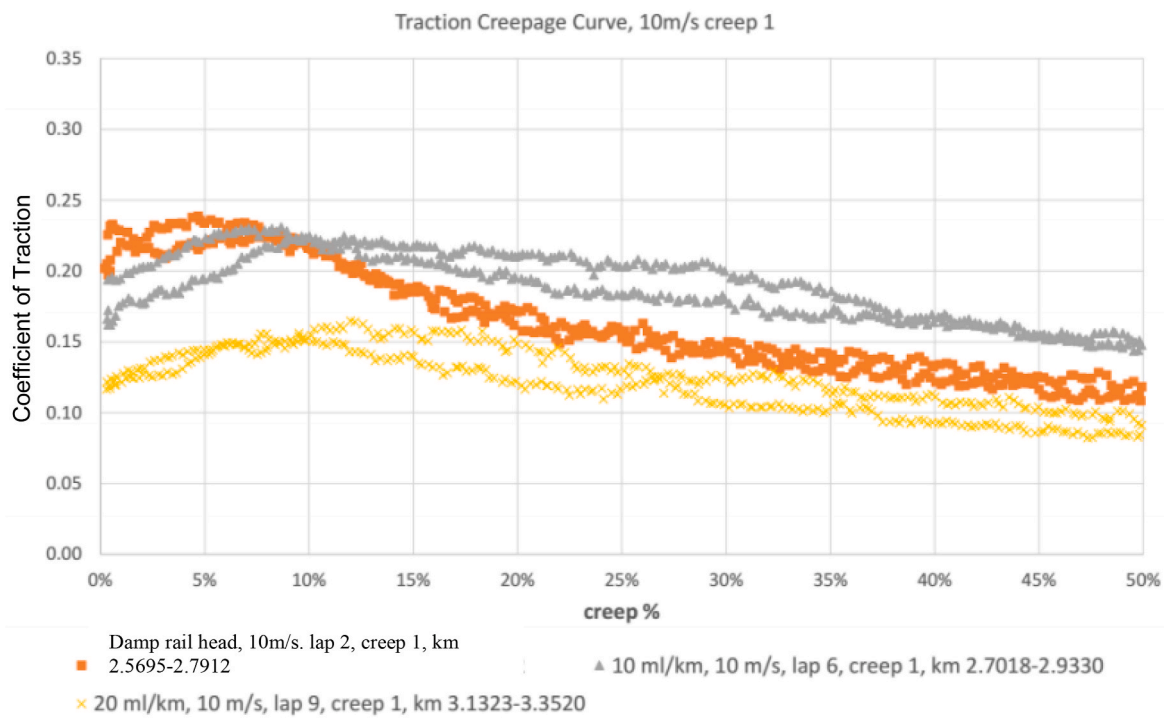


Fig. 12. Field test data for runs with and without TOR FMs at Dosages of 10 and 20 mL/km (16.1 and 32.2 mL/mile).

and a temperature dependent value ( $T$ ) as shown in Table 2.

The routines for parameterisation of the ECF model also contain a parameter representing the equivalent inverse stiffness of the test-rig ( $L_x$ ). This is necessary as the third-body layer is very thin and therefore has high stiffness. Compared to this stiffness, the flexibility of the rig is generally significant and therefore must be accounted for. Note that it is only used in the parameterisation process and is not an input to the model. Meierhofer [37] found that values for inverted elastic stiffness,  $L_e$ , made no significant difference to the traction characteristics, unless it was changed by an order of magnitude. It is also difficult to separate  $L_e$

from  $L_x$ . To simplify the optimization process,  $L_e^0$ , was calculated using the shear modulus of steel ( $G_s = 79.3$  GPa) and a mean thickness for a third-body layer of  $20 \mu\text{m}$  (identified from Ref. [45]). Meierhofer parameterised the ECF model using data from dry HPT tests (on a different rig to this work) and using temperatures from vehicle tests [37]. The HPT interface does not rise enough above ambient to be used for this.

Starting from the parameters derived by Meierhofer [37], the optimization routine was then allowed to optimize for  $L_0$ ,  $L_p$  and  $L_x$ .  $L_e$  values are not optimized. The resulting ECF parameter values and plots are shown in Table 3 and Fig. 14 respectively. The rig stiffness was

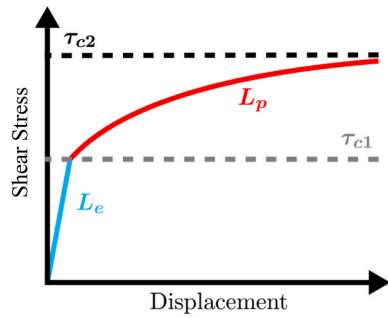


Fig. 13. Material parameters required for ECF model [37].

**Table 2**  
Arrangement of constants used to define the behaviour of a third-body layer in the ECF model.

Material parameter	Nominal	Pressure dependency coefficients	Temperature dependency coefficients
Inverted stiffness ( $L_e$ )	$L_e^0$	$L_e^p$	$L_e^T$
Plasticity factor ( $L_p$ )	$L_p^0$	$L_p^p$	$L_p^T$
First critical shear stress ( $t_{c1}$ )	$t_{c1}^0$	$t_{c1}^p$	$t_{c1}^T$
Second critical shear stress ( $t_{c2}$ )	$t_{c2}^0$	$t_{c2}^p$	$t_{c2}^T$

**Table 3**  
ECF input parameters for dry baseline.

Material parameter	Nominal	Pressure dependency coefficients
$L_e$	$0.25 \frac{\mu m}{GPa}$	$\infty \frac{1}{GPa}$
$L_p$	$0.0602 \text{ mm}$	$1.52 \frac{1}{GPa}$
$t_{c1}$	$4.18 \text{ GPa}$	$0.0778 \frac{1}{GPa}$
$t_{c2}$	$1.90 \text{ GPa}$	$0.0455 \frac{1}{GPa}$

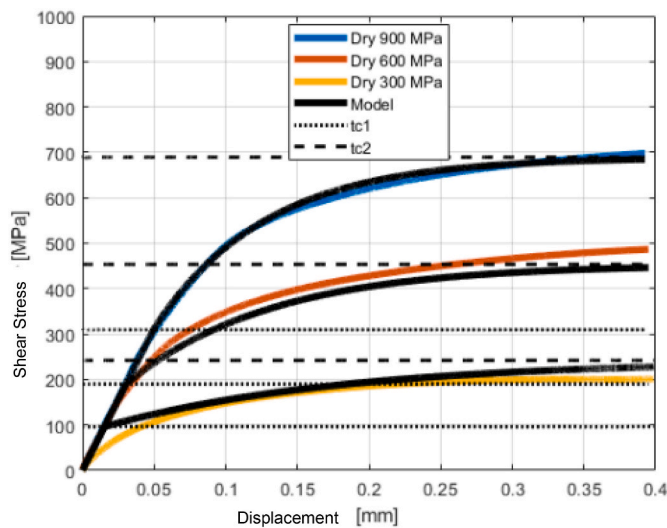


Fig. 14. ECF fit for dry baseline tests at three pressures: 300, 600 and 900 MPa.

optimized to find an estimated flexibility of  $L_x = 160 \mu\text{m}/\text{GPa}$ , equivalent to  $ST = 0.163 \text{ deg}/\text{kNm}$ . An error value of  $= 5.22\%$  was achieved.

The rig flexibility used appeared to produce a suitable stiffness characteristic for the elastic part of the model. This value was therefore used for all subsequent parameterisations. While the dry baseline tests were carried out at three different normal pressures, subsequent tests were only run at one. Therefore, only the nominal values were optimized for the TOR FM tests. Pressure dependency values from the dry tests were used for these.

As an example, the ECF fit for the TOR FM dosage of 16 mL/mile is shown in Fig. 15. An error value of 4.87% was achieved (the root mean square error (RMSE) was calculated:  $\text{RMSE} = \sqrt{(\text{mean}((\kappa - \kappa_p)^2))}$ , where  $\kappa_p$  is the model prediction and  $\kappa$  the measured value. To avoid unit dependencies, the relative error,  $\epsilon$ , was calculated by using the coefficient of variation of the RSME ( $\text{CV}(\text{RMSE})$ ):  $\epsilon = \text{CV}(\text{RMSE}) = 100 \times (\text{RMSE}/\text{mean}\kappa)$ ). The same process was undertaken for wet tests as well as all the TOR FM dosages tested in the HPT rig.

Fig. 16 presents the creep curves calculated with the ECF model representing all assessed materials for the locomotive wheel/rail interface conditions to allow a comparison with the field data shown in Fig. 12. The water curve was parameterised using data from tests carried out in a previous project [46]. The results are largely as would be expected, with traction coefficients tending to decrease with increasing dosages of TOR FM. For 512 mL/mile and 2048 mL/mile dosages, the input parameters are very similar, resulting in almost identical creep curves for both the full-scale contacts.

The peak traction coefficient and the traction coefficient at 20% slip have been compared in Table 4. As mentioned earlier, whilst the intended “dry” field data was measured on a very damp day, with occasional drizzle; for this reason, the results have been compared with the wet ECF prediction rather than the dry prediction. The 16 and 32 mL/mile TOR FM dosages modelled are equivalent to the 10 and 20 mL/km dosages used in the track trials, respectively. Experimental data is lacking at very low creep values, making it impossible to calculate a value for the initial gradient, however, it can be seen that both the experimental and predicted traction results are nearing their peak values at creepage values lower than 10%.

Given the nature of the field trials, the outcomes compare very well. However, the peak traction values appear to have been very slightly underestimated in all three of the cases. For the wet case, the ECF model has correctly predicted the creepage value of the peak coefficient of traction, and the coefficient of traction at 20% creep is also very similar; this suggests the temperature dependency parameters are correctly set to model the friction drop in this case. For the two TOR FM cases, the

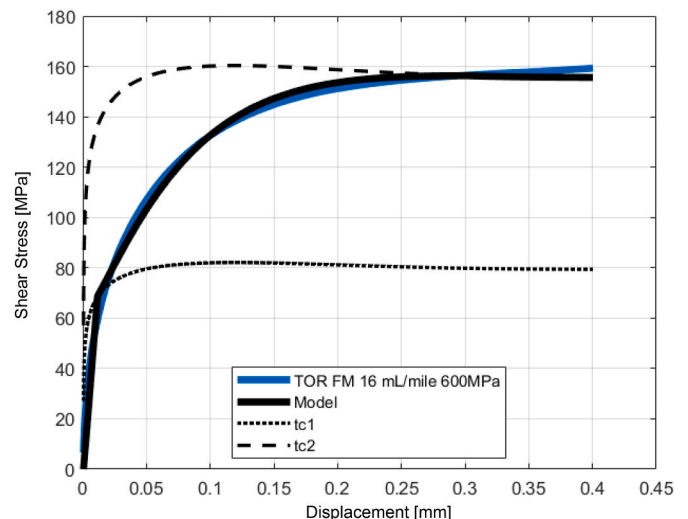


Fig. 15. ECF fit for TOR FM 16 mL/mile dosage at 600 MPa.

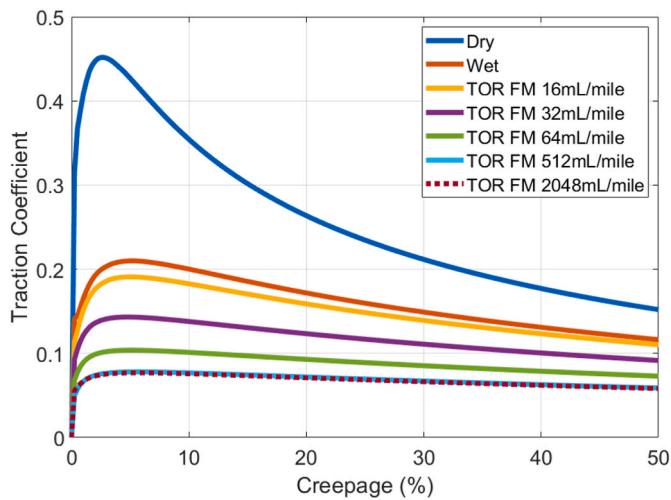


Fig. 16. ECF creep curves for dry (no TOR FM applied), wet (no TOR FM applied) and TOR FM cases.

Table 4  
ECF prediction versus loco test data.

Factor	Case	ECF Model	Loco Test
Gradient of initial slope	All	1.25	–
Peak coeff. of traction	Dry (no TOR FM applied)	0.45 (@2.6%)	–
	Wet (no TOR FM applied)	0.21 (@5.1%)	0.24 (@5%)
	TOR FM 16mL/mile	0.19 (@5%)	0.23 (@5%)
	TOR FM 32 mL/mile	0.14 (@4.8%)	0.16 (@12%)
Traction at 20% slip	Dry (no TOR FM applied)	0.26	–
	Wet (no TOR FM applied)	0.17	0.17
	TOR FM 16mL/mile	0.16	0.20
	TOR FM 32 mL/mile	0.12	0.14

temperature dependency coefficients appear to overestimate the effect of temperature on the coefficient of traction, which continues to rise until higher creeps in the experimental cases. This is perhaps not surprising as the temperature dependency coefficients have been established using data for wet conditions; temperature dependency coefficients have not been produced for TOR FM conditions, therefore, wet condition behaviour has been assumed.

7. Discussion

An alternative method for assessing TOR FM performance has been presented that offers advantages over the more traditional twin-disc type testing approach.

TOR products offer many challenges for testing. The main reason is that they have very diverse properties. TOR lubricants based on oils and greases are perhaps a little easier to apply and test. The water-based TOR FMs however, present some issues. Where they are applied they are wet, but as they are spread down the rail they dry out and mix with the natural third-body layer which leaves the layer with varying properties. This results in the layer giving different creep force behaviour as distance down the rail from the application point increases (see Fig. 17 [47]). This test method offers a means to study how the creep force properties of this transient layer vary, but only if a dry layer can be applied rather than a wet layer (a “wet” product test is only relevant for the point of application). Other work on the application of water-based TOR products found that low friction coefficients were obtained [34].

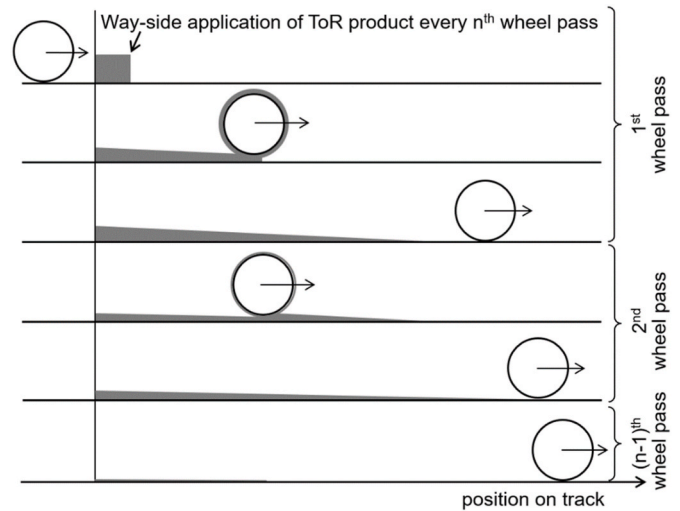


Fig. 17. Schematic of way-side application of TOR products. Product is spread along the track and consumed by passing wheels. Product heights (in grey) are exaggerated [47].

This may have been because of issues with the application and layer formation. Here intermediate levels of friction were generated as would be expected at the typical application amounts.

The approach used here has worked, data from the tests has led to successful full-scale predictions. There were, however, some issues. Despite an effort to spread the dilutions across the whole of the contact, it was found that the solid particles agglomerated during the evaporation process. This adds inconsistencies to testing, as the TOR FM is not spread evenly throughout the contact. To prevent this agglomeration occurring it is suggested to apply 400 µL of distilled water to the surface and then apply the 400 µL of dilution. This produces a more even spread of TOR FM compared to the original 400 µL of dilution and 800 µL of dilution as shown in Fig. 18. The reason for this is that the original 400 µL is not enough liquid to completely cover the surface of the specimen and so the water evaporated from the edges faster than the centre. Whereas, with 800 µL of liquid applied, the applied dilution filled the specimen area and dried evenly.

In this work it was critical to be able to provide field validation which is often unachievable due to cost or availability of appropriate facilities/instrumented vehicles. The locomotive data was very close to that predicted by the ECF approach parameterised using the HPT test data. This shows the usefulness of the ECF model to predict friction for different third-body layers. There are many more that could be considered now to build-up its capabilities.

8. Conclusions

This work has.

- Developed and application method for generating TOR FM layers on HPT specimens
- Developed an alternative test method for assessing TOR FM friction characteristics that offers advantages over traditional “recycling” contact methods such as used by Twin-disc testing
- Showed via the HPT testing that there is a threshold value, above which increasing the application amount does not reduce the friction coefficient (an important characteristic for TOR FM).
- Improved the capability of the ECF model to include TOR FM characteristics
- Provided validation for the ECF model predictions from locomotive data from a field study

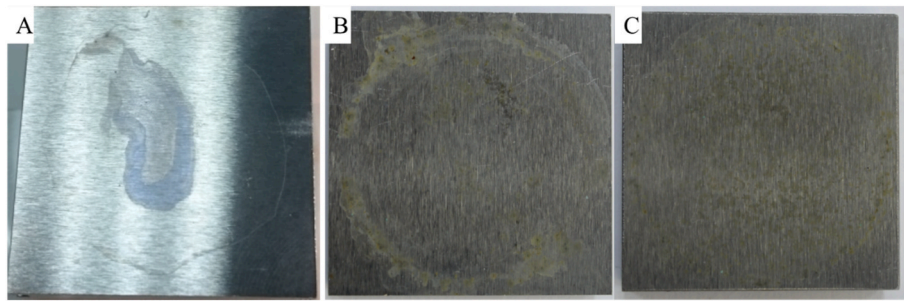


Fig. 18. TOR FM at 32 mL/mile dilution A) original 400 µL dilution, B) 800 µL dilution, C) 400 µL of distilled water followed by 400 µL of dilution.

The testing/modelling framework can be expanded to build-in the influence of other third-body materials now to generate creep force behaviour to implement in multi-body dynamics simulations to understand their effect on train behaviour, but also in damage modelling.

#### Author contribution

Roger Lewis: Supervisor; Conceptualisation; Project Administration; Investigation; Methodology; Writing – review and editing.

Klaus Six: Conceptualisation; Investigation; Methodology; Writing – review and editing.

Alexander Meierhofer: Writing – review and editing.

Martin Evans: Investigation; Methodology; Writing – original draft.

Zing Lee: Writing – original draft.

Matthew Harmon: Writing – original draft.

Dmitry Gutsulyak: Investigation; Methodology.

Richard Stock: Investigation; Methodology.

The authors confirm that this is original work and the paper has not been submitted elsewhere for publication.

#### Declaration of competing interest

The authors declare the following financial interests/personal relationships which may be considered as potential competing interests: Martin Evans reports financial support was provided by L.B. Foster.

#### Data availability

Data will be made available on request.

#### Acknowledgements

The authors would like to acknowledge the funding provided for the work by L.B. Foster for the PhD carried out by Martin Evans.

The work was also supported by the EPSRC Programme Grant “Friction: The Tribology Enigma” (EP/R001766/1).

The authors would like to acknowledge the financial support within the COMET K2 Competence Centers for Excellent Technologies from the Austrian Federal Ministry for Climate Action (BMK), the Austrian Federal Ministry for Digital and Economic Affairs (BMDW), the Province of Styria (Dept. 12) and the Styrian Business Promotion Agency (SFG). The Austrian Research Promotion Agency (FFG) has been authorised for the programme management. They would furthermore like to express their thanks to their supporting industrial and scientific project partners Siemens Mobility GmbH, voestalpine Rail Technologies GmbH, L.B. Foster, SBB Infrastructure, Virtual Vehicle Research GmbH, and the University of Sheffield.

For the purpose of open access, the author has applied a Creative Commons Attribution (CC BY) license to any Author Accepted Manuscript version arising.

#### References

- [1] S. Aldajah, O.O. Aljayi, G.R. Fenske, S. Kumar, Investigation of top of rail lubrication and laser glazing for improved railroad energy efficiency, *J. Tribol.* 125 (3) (2003) 643.
- [2] D.T. Eadie, M. Santoro, Top-of-Rail friction control for curve noise mitigation and corrugation rate reduction, *J. Sound Vib.* 293 (2006) 747–757.
- [3] D.T. Eadie, M. Santoro, J. Kalousek, Railway noise and the effect of top of rail liquid friction modifiers: changes in sound and vibration spectral distributions in curves, *Wear* 258 (No. 7–8) (2005) 1148–1155.
- [4] R. Galas, M. Omasta, M. Klapka, S. Keawunruen, I. Krupka, M. Hartl, Case study: the influence of oil-based friction modifier quantity on tram braking distance and noise, *Tribology* 39 (2017) 198–206.
- [5] X. Liu, P.A. Meehan, Investigation of squeal noise under positive friction characteristics condition provided by friction modifiers, *J. Sound Vib.* 371 (2016) 393–405.
- [6] P.A. Meehan, X. Liu, Modelling and mitigation of wheel squeal noise under friction modifiers, *J. Sound Vib.* 440 (2018) pp147–p160.
- [7] D. Kvarda, S. Skurka, R. Galas, M. Omasta, L.B. Shi, H.H. Ding, W.-J. Wang, I. Krupka, M. Hartl, The effect of top of rail lubricant composition on adhesion and rheological behaviour, *Int. J. Eng. Sci. Technol.* 35 (2021), 101100.
- [8] R. Galas, D. Kvarda, M. Omasta, I. Krupka, M. Hart, The role of constituents contained in water-based friction modifiers for top-of-rail application, *Tribol. Int.* 117 (2018) 87–97.
- [9] Q. Li, B.N. Wu, H.H. Ding, R. Galas, D. Kvarda, Q.Y. Liu, Z.R. Zhou, M. Omasta, W.-J. Wang, Numerical prediction on the effect of friction modifiers on adhesion behaviours in the wheel-rail starved EHL contact, *Tribol. Int.* 170 (2022), 107519.
- [10] B.N. Wu, L.B. Shi, H.H. Ding, J. Guo, Q.Y. Liu, Z.R. Zhou, R. Lewis, W.-J. Wang, Influence of different solid particles in friction modifier on wheel-rail adhesion and damage behaviours, *Wear* 522 (2023), 204833.
- [11] W.J. Wang, T.F. Liu, H.Y. Wang, Q.Y. Liu, M.H. Zhu, X.S. Jin, Influence of friction modifiers on improving adhesion and surface damage of wheel/rail under low adhesion conditions, *Tribol. Int.* 75 (2014) 16–23.
- [12] X. Lu, T.W. Makowsky, D. Eadie, Friction management on a Chinese heavy haul coal line, *Journal of Rail and Rapid Transit, Proceedings of IMechE Part F* 226 (No. 6) (2012) 630–640.
- [13] D. Elvidge, R. Stock, C. Hardwick, K. Oldknow, The effect of freight train mounted TOR-FM on wheel life and defects, in: *Proceedings of the Third International Conference on Railway Technology: Research, Development and Maintenance*, vols. 5–8, 2016, pp. 8–12. Cagliari, Italy.
- [14] D.V. Gutsulyak, L.J.E. Stanlake, H. Qi, Twin disc evaluation of third body materials in the wheel/rail interface, *Tribol. Mater. Surface Interfac.* 15 (2020) 115–126.
- [15] D.T. Eadie, M. Santoro, K. Oldknow, Y. Oka, Field studies of the effect of friction modifiers on short pitch corrugation generation in curves, *Wear* 265 (9–10) (2008) pp.1212–1221.
- [16] S.L. Grassie, Rail corrugation: advances in measurement, understanding and treatment, *Wear* 258 (No. 7–8) (2005) 1224–1234.
- [17] D.T. Eadie, J. Kalousek, K.C. Chiddick, The role of high positive friction (HPF) modifier in the control of short pitch corrugations and related phenomena, *Wear* 253 (1–2) (2002) 185–192.
- [18] C. Hardwick, R. Lewis, R. Stock, The effects of friction management materials on rail with pre-existing RCF surface damage, *Wear* 384–385 (2017) 50–60.
- [19] D.T. Eadie, D. Elvidge, K. Oldknow, R. Stock, P. Pointner, J. Kalousek, P. Klausner, The effects of top of rail friction modifier on wear and rolling contact fatigue: full-scale rail-wheel test rig evaluation, analysis and modelling, *Wear* 265 (No. 9–10) (2008), 1222–230.
- [20] M. Chestney, N. Dadkash, D.T. Eadie, The effect of top of rail friction control on a European passenger system: the heathrow express experience, *Proceedings of the 8th International Conference on Contact Mechanics and Wear of Rail/Wheel Systems 2* (2009) 591–598. Florence, Italy, 15–18 September.
- [21] C. Hardwick, S.R. Lewis, R. Lewis, The effect of friction modifiers on wheel/rail isolation at low axle loads, *Journal of Rail and Rapid Transit, Proceedings of the IMechE Part F* 228 (No. 7) (2014) 768–783.
- [22] RSSB, Stage 2 Development of the Vehicle Track Interaction Strategic Model”, 2013. RSSB report on project T792.
- [23] M. Evans, W.A. Skipper, L. Buckley-Johnstone, A. Meierhofer, K. Six, R. Lewis, The development of a high pressure torsion test methodology for simulating wheel/rail contacts, *Tribol. Int.* 156 (2021), 106842.

- [24] R. Stock, L. Stanlake, C. Hardwick, M. Yu, D. Eadie, R. Lewis, Material concepts for top of rail friction management – classification, characterisation and application, *Wear* 366–367 (2016) 225–232.
- [25] X. Lu, J. Cotter, D.T. Eadie, Laboratory study of the tribological properties of friction modifier thin films for friction control at the wheel/rail interface, *Wear* 259 (No. 7–12) (2005) 1262–1269.
- [26] L. Buckley-Johnstone, M. Harmon, C. Hardwick, R. Stock, R. Lewis, A comparison of friction modifier performance using two laboratory scale tests, *Journal of Rail and Rapid Transit, Proceedings of the IMechE, Part F* 233 (2018) 201–210.
- [27] R. Stock, D. Eadie, K. Oldknow, Rail grade selection and friction management: a combined approach for optimising rail-wheel contact, *Ironmak. Steelmak.* 40 (No. 2) (2013) 108–114.
- [28] R. Stock, D.T. Eadie, D. Elvidge, K. Oldknow, Influencing rolling contact fatigue through top of rail friction modifier application - a full scale wheel-rail test rig study, *Wear* 271 (No. 1–2) (2011) 134–142.
- [29] D. Kvarda, R. Galas, M. Omasta, L.B. Shi, H.H. Ding, W.-J. Wang, L. Krupka, M. Hartl, Asperity-based model for prediction of traction in water-contaminated wheel-rail contact, *Tribol. Int.* 157 (2021), 106900.
- [30] K. Matsumoto, Y. Suda, T. Fujii, H. Komines, M. Tomeoka, Y. Satoh, T. Nakai, M. Tanimoto, Y. Kishimoto, The optimum design of an onboard friction control system between wheel and rail in a railway system for improved curving negotiation, *Veh. Syst. Dyn.* 44 (Supplement) (2006) 531–540.
- [31] D. Davis, Effectiveness of New Friction Control Materials – Vehicle Track Systems Research”, Presentation at Annual AAR Research Review, 2015. March 31st - April 1st 2015.
- [32] W.A. Skipper, S. Nadimi, A. Chalisey, R. Lewis, Particle characterisation of rail sands for understanding tribological behaviour, *Wear* 432–433 (2019), 202960.
- [33] L.E. Buckley-Johnstone, G. Trummer, P. Voltr, A. Meierhofer, K. Six, D.I. Fletcher, R. Lewis, Assessing the impact of small amounts of water and iron oxides on adhesion in the wheel/rail interface using high pressure torsion testing, *Tribol. Int.* 135 (2019) 55–64.
- [34] D. Kvarda, R. Gala, M. Omsasta, M. Hartl, I. Krupka, M. Dzimko, Shear properties of top-of-rail products in numerical modelling, in: *Journal of Rail and Rapid Transit, Proceedings of the IMechE Part F*, 2022.
- [35] L. Buckley-Johnstone, R. Lewis, D. Fletcher, K. Six, G. Trummer, A. Meierhofer, T1077: Modelling & Quantifying the Influence of Water on Wheel/Rail Adhesion Levels”, 2015 (London, UK).
- [36] E. Vollebregt, K. Six, O. Polach, Challenges and progress in the understanding and modelling of the wheel–rail creep forces, *Veh. Syst. Dyn.: International Journal of Vehicle Mechanics and Mobility* 59 (No. 7) (2021) 1026–1068.
- [37] A. Meierhofer, A New Wheel-Rail Creep Force Model Based on Elasto-Plastic Third Body Layers”, PhD Thesis, Graz University of Technology, 2015, 2015.
- [38] K. Six, A. Meierhofer, G. Müller, P. Dietmaier, Physical processes in wheel-rail contact and its implications on vehicle–track interaction, *Veh. Syst. Dyn.* 53 (No. 5) (2014) 635–650.
- [39] C. Tomberger, P. Dietmaier, W. Sextro, K. Six, Friction in wheel-rail contact: a model comprising interfacial fluids, surface roughness and temperature, *Wear* 271 (No. 1–2) (2011) 2, 12.
- [40] J. Kalker, A fast algorithm for the simplified theory of rolling contact, *Veh. Syst. Dyn.* 11 (1982) 1–13.
- [41] K. Six, A. Meierhofer, G. Trummer, C. Bernsteiner, Plasticity in wheel-rail contact and its implications on vehicle-track interaction, *Journal of Rail and Rapid Transit, Proceedings of the IMechE Part F* 231 (No. 5) (2017) 558–569.
- [42] S. Alexandrov, A property of equations of rigid/plastic material obeying a voce-type hardening law, *Meccanica* 34 (1999) 349–356.
- [43] A. Meierhofer, G. Trummer, C. Bernsteiner, K. Six, Vehicle tests showing how the weather in autumn influences the wheel-rail traction characteristics, *Journal of Rail and Rapid Transit, Proceedings of the IMechE Part F* 234 (No. 4) (2020) 426–435.
- [44] R. Lewis, E.A. Gallardo, T. Hilton, T. Armitage, Effect of oil and water mixtures on adhesion in the wheel/rail contact, *Journal of Rail and Rapid Transit, Proceedings of the IMechE Part F* 223 (2009) 275–283.
- [45] A. Meierhofer, C. Hardwick, R. Lewis, K. Six, P. Dietmaier, Third body layer - experimental results and a model describing its influence on the traction coefficient, *Wear* 314 (2014) 148–154.
- [46] M.E. Evans, Performance Assessment of Friction Management Products in the Wheel-Rail Interface”, PhD Thesis, The University of Sheffield, UK, 2018.
- [47] G. Trummer, Z.S. Lee, R. Lewis, K. Six, Modelling of frictional conditions in the wheel/rail interface due to application of top-of-rail products, *Lubricants* 9 (10) (2021).